A Semi-analytical Solutions of Elastic Stress in Circular Rock Stratum Based on the Theory of Curved Beam

Wankui Bu, Hui Xu

***Abstract*—Circular rock stratum is inevitably encountered in underground mining engineering, resulting in waste of resources and dynamic instability. Based on the elastic theory of curved beam and finite difference computation, a displacement function is proposed in polar coordinates to solve two partial differential equations with the boundary conditions in elastic, isotropic and homogeneous rock. A semi-analytical solution of elastic stress in circular rock stratum is obtained according to the governing equation and stress components in the form of displacement function. In addition, the variations of stress distribution with different influencing factors are analyzed, which is helpful to a better understanding of the stability of circular stratum after coal extractions. Moreover, this semi-analytical elastic stress solution is applied to the fold structure in No.2502 mining area. Last but not the least, the dangerous positions in the process of coal extractions are pointed out for the safety and better construction in coal mine engineering.**

***Index Terms*—Circular rock stratum, Displacement function, Elastic mechanics, Elastic stress solution**

I. INTRODUCTION

Coal resources have always been and will be the main energy for a long time in China, accounting for about 70% of the disposable energy structure [1]–[2]. However, a considerable part of coal resources exist in continuous circular rock strata, which are threatened by dynamic instability during the coal extractions. The common characteristics of circular rock stratum are the existence of curvature and horizontal tectonic stress in the stratum, which will at least lead to elastic deformation during the coal mining. Different from the horizontal layered stratum, understanding the elastic stress distribution in circular stratum after coal extractions is great significant to the underground mining engineering. Although the visual stress solution of circular rock stratum can be obtained by numerical simulation, the analytical solution of circular rock stratum provides insight into the general properties of the solution. On the other hand, the mining engineers should be able to evaluate the general correctness of numerical analysis due to the simplification of numerical modeling, however, analytical solution provides a valuable method for this evaluation. Therefore, the elastic stress distribution in circular rock stratum may become an important research topic for mining engineers.

Traditionally, the stress function formula and displacement function formula are two common methods for stress analysis of curved beams in elastic mechanics. The former is the simplest method for curved beams in elastic mechanics, and the stress solutions of curved beams with different cross sections or with different loading have been obtained in literatures [3]–[10] as well as the improving calculation method. However, when the boundary condition is displacement condition or strain condition, a satisfactory solution cannot be obtained. As for the latter, it is difficult to solve the two partial differential equations of radial displacement (horizontal displacement) and circumferential displacement (vertical displacement), so it is not widely used in geotechnical engineering. Especially when the boundary condition is the mixed mode of displacement (strain) and loading (stress), it is impossible to obtain the exact solution from two variable coefficient partial differential equations. Therefore, these traditional methods seem to be inaccurate and unreliable for these mixed boundary value problems [11]–[13]. Besides, the Hamiltonian system is introduced into the elastic problems and the Symplectic Elasticity is established, which has the defect of breaking in the Jordan chain [14].

In recent years, the combination of elasticity and computational mechanics have been used to solve mixed boundary conditions. The common methods for numerical calculation are the Finite Element Method (FEM) and the Finite Difference Method (FDM). FEM has been successfully and widely applied in stress analysis [15]–[18], however, the large bending deformation in FEM results are unreliable [19]. In addition, it is proved that the calculation results of FDM are better than that of FEM [20]–[25].

Based on the above considerations, a displacement function is given in polar coordinate system to solve partial differential equations with two mixed boundary conditions in elastic, isotropic and homogeneous rock. Then, the radial and circumferential displacement are expressed as a summation of all possible partial derivatives of the displacement function up to an order of two, together with the unknown coefficients. The displacement function and its numerical solution are obtained by the finite difference computation. Meanwhile, the variations of stress distribution with different influencing factors are analyzed according to the analytical expression of stress components in the form of displacement function.

Manuscript received September 16, 2021; revised May 7, 2022.

This work was supported by Shandong Provincial Natural Science Foundation (Project ZR2020ME100) and Heze University Natural Science Foundation (Project XY21BS42).

Wankui Bu is a Professor of College of Urban Construction, Heze University, Heze, 274015, China (corresponding author, phone: 086-0530-5525153; e-mail: bwk239@126.com).

Hui Xu is an Associate Professor of Editorial Department, Heze University, Heze, 274015, China (corresponding author, phone: 086-0530-5525336; e-mail: xu_hui521@126.com).

Finally, these semi-analytical elastic stress solutions are applied to the fold structure in No.2502 mining area in China.

II. Elastic Stress Solutions for Circular Rock Stratum

A. Governing Equation in the Form of Displacement Function

According to elastic mechanics in polar coordinate system (r, θ) [4], the equilibrium equations in the form of radial displacement u_r and circumferential displacement u_θ in plane problem without external force are as follows.

$$\frac{\partial^2 u_r}{\partial r^2}+\frac{1}{2r(1-\mu)}\frac{\partial^2 u_\theta}{\partial r\partial\theta}+\frac{(1-2\mu)}{2r^2(1-\mu)}\frac{\partial^2 u_r}{\partial\theta^2}+\frac{1}{r}\frac{\partial u_r}{\partial r}-\frac{(3-4\mu)}{2r^2(1-\mu)}\frac{\partial u_\theta}{\partial\theta}-\frac{u_r}{r^2}=0 \tag{1a}$$

$$\begin{aligned}&\frac{(1-2\mu)}{2(1-\mu)}\frac{\partial^2 u_\theta}{\partial r^2}+\frac{1}{2r(1-\mu)}\frac{\partial^2 u_r}{\partial r\partial\theta}+\frac{1}{r^2}\frac{\partial^2 u_\theta}{\partial\theta^2}+\frac{(1-2\mu)}{2r(1-\mu)}\frac{\partial u_\theta}{\partial r}+\\&\frac{(3-4\mu)}{2r^2(1-\mu)}\frac{\partial u_r}{\partial\theta}-\frac{(1-2\mu)}{2r^2(1-\mu)}u_\theta=0\end{aligned} \tag{1b}$$

Where, u_θ and u_r are the circumferential displacement and radial displacement, respectively, and μ is the Poisson's ratio.

Equation (1) gives two partial differential equations in plane strain problem in polar coordinate system. The exact solutions of radial and circumferential displacement should satisfy the two equations and all boundary conditions. However, these equations are simultaneous partial differential equations with variable coefficients. Moreover, boundary conditions are in mixed type of displacement (strain) and loading (stress). Thus, the exact results in this case are impossible. The mathematical method can be adopted to reduce variables. The feasible option is to change two equations with two variables into one equation with a single variable.

In order to reduce the two equations with two variables in (1) to one equation with a single variable, a displacement function $\psi(r, \theta)$ is introduced, and the radial and circumferential displacement are expressed as follows.

$$u_r=\alpha_1\frac{\partial^2\psi}{\partial r^2}+\alpha_2\frac{1}{r}\frac{\partial^2\psi}{\partial r\partial\theta}+\alpha_3\frac{1}{r^2}\frac{\partial^2\psi}{\partial\theta^2}+\alpha_4\frac{1}{r}\frac{\partial\psi}{\partial r}+\alpha_5\frac{1}{r^2}\frac{\partial\psi}{\partial\theta}+\alpha_6\frac{1}{r^2}\psi \tag{2a}$$

$$u_\theta=\alpha_7\frac{\partial^2\psi}{\partial r^2}+\alpha_8\frac{1}{r}\frac{\partial^2\psi}{\partial r\partial\theta}+\alpha_9\frac{1}{r^2}\frac{\partial^2\psi}{\partial\theta^2}+\alpha_{10}\frac{1}{r}\frac{\partial\psi}{\partial r}+\alpha_{11}\frac{1}{r^2}\frac{\partial\psi}{\partial\theta}+\alpha_{12}\frac{1}{r^2}\psi \tag{2b}$$

Where, coefficients α_i (i=1,2,3,…,12) are defined as material constants [22].

Substituting the above expressions of u_r and u_θ into (1), two partial differential equations in the form of displacement function can be represented as follows.

$$\begin{aligned}&\alpha_1\frac{\partial^4\psi}{\partial r^4}+\frac{1}{r}\left\{\alpha_2+\frac{1}{2(1-\mu)}\alpha_7\right\}\frac{\partial^4\psi}{\partial r^3\partial\theta}+\frac{1}{r^2}\left\{\frac{1-2\mu}{2(1-\mu)}\alpha_1+\alpha_3+\frac{1}{2(1-\mu)}\alpha_8\right\}\frac{\partial^4\psi}{\partial r^2\partial\theta^2}\\&+\frac{1}{r^3}\left\{\frac{1-2\mu}{2(1-\mu)}\alpha_2+\frac{1}{2(1-\mu)}\alpha_9\right\}\frac{\partial^4\psi}{\partial r\partial\theta^3}+\frac{1}{r^4}\left\{\frac{1-2\mu}{2(1-\mu)}\alpha_3\right\}\frac{\partial^4\psi}{\partial\theta^4}+\frac{1}{r}\{\alpha_1+\alpha_4\}\frac{\partial^3\psi}{\partial r^3}\\&+\frac{1}{r^2}\left\{-\alpha_2+\alpha_5-\frac{3-4\mu}{2(1-\mu)}\alpha_7+\frac{1}{2(1-\mu)}\alpha_{10}\right\}\frac{\partial^3\psi}{\partial r^2\partial\theta}\\&+\frac{1}{r^3}\left\{-3\alpha_3+\frac{1-2\mu}{2(1-\mu)}\alpha_4-2\alpha_8+\frac{1}{2(1-\mu)}\alpha_{11}\right\}\frac{\partial^3\psi}{\partial r\partial\theta^2}\\&+\frac{1}{r^4}\left\{\frac{1-2\mu}{2(1-\mu)}\alpha_5+\frac{-5+4\mu}{2(1-\mu)}\alpha_9\right\}\frac{\partial^3\psi}{\partial\theta^3}+\frac{1}{r^2}\{-\alpha_1-\alpha_4+\alpha_6\}\frac{\partial^2\psi}{\partial r^2}\\&+\frac{1}{r^3}\left\{-3\alpha_5-2\alpha_{10}+\frac{1}{2(1-\mu)}\alpha_{12}\right\}\frac{\partial^2\psi}{\partial r\partial\theta}+\frac{1}{r^4}\left\{3\alpha_3+\frac{1-2\mu}{2(1-\mu)}\alpha_6-\frac{5-4\mu}{2(1-\mu)}\alpha_{11}\right\}\frac{\partial^2\psi}{\partial\theta^2}\\&+\frac{1}{r^3}\{-3\alpha_6\}\frac{\partial\psi}{\partial r}+\frac{1}{r^4}\left\{3\alpha_5-\frac{5-4\mu}{2(1-\mu)}\alpha_{12}\right\}\frac{\partial\psi}{\partial\theta}+\frac{1}{r^4}\{3\alpha_6\}\psi=0\end{aligned} \tag{3a}$$

$$\begin{aligned}&\frac{1-2\mu}{2(1-\mu)}\alpha_7\frac{\partial^4\psi}{\partial r^4}+\frac{1}{r}\left\{\frac{1}{2(1-\mu)}\alpha_1+\frac{1-2\mu}{2(1-\mu)}\alpha_8\right\}\frac{\partial^4\psi}{\partial r^3\partial\theta}\\&+\frac{1}{r^2}\left\{\frac{1}{2(1-\mu)}\alpha_2+\alpha_7+\frac{1-2\mu}{2(1-\mu)}\alpha_9\right\}\frac{\partial^4\psi}{\partial r^2\partial\theta^2}+\frac{1}{r^3}\left\{\frac{1}{2(1-\mu)}\alpha_3+\alpha_8\right\}\frac{\partial^4\psi}{\partial r\partial\theta^3}\\&+\frac{1}{r^4}\{\alpha_9\}\frac{\partial^4\psi}{\partial\theta^4}+\frac{1}{r}\left\{\frac{1-2\mu}{2(1-\mu)}\alpha_7+\frac{1-2\mu}{2(1-\mu)}\alpha_{10}\right\}\frac{\partial^3\psi}{\partial r^3}\\&+\frac{1}{r^2}\left\{\frac{3-4\mu}{2(1-\mu)}\alpha_1+\frac{1}{2(1-\mu)}\alpha_4-\frac{1-2\mu}{2(1-\mu)}\alpha_8+\frac{1-2\mu}{2(1-\mu)}\alpha_{11}\right\}\frac{\partial^3\psi}{\partial r^2\partial\theta}\\&+\frac{1}{r^3}\left\{\frac{1-2\mu}{1-\mu}\alpha_2+\frac{1}{2(1-\mu)}\alpha_5-\frac{3(1-2\mu)}{2(1-\mu)}\alpha_9+\alpha_{10}\right\}\frac{\partial^3\psi}{\partial r\partial\theta^2}\\&+\frac{1}{r^4}\left\{\frac{1-4\mu}{2(1-\mu)}\alpha_3+\alpha_{11}\right\}\frac{\partial^3\psi}{\partial\theta^3}+\frac{1}{r^2}\left\{-\frac{1-2\mu}{2(1-\mu)}\alpha_7-\frac{1-2\mu}{2(1-\mu)}\alpha_{10}+\frac{1-2\mu}{2(1-\mu)}\alpha_{12}\right\}\frac{\partial^2\psi}{\partial r^2}\\&+\frac{1}{r^3}\left\{\frac{1-2\mu}{1-\mu}\alpha_4+\frac{1}{2(1-\mu)}\alpha_6-\frac{3(1-2\mu)}{2(1-\mu)}\alpha_{11}\right\}\frac{\partial^2\psi}{\partial r\partial\theta}\\&+\frac{1}{r^4}\left\{\frac{1-4\mu}{2(1-\mu)}\alpha_5+\frac{3(1-2\mu)}{2(1-\mu)}\alpha_9+\alpha_{12}\right\}\frac{\partial^2\psi}{\partial\theta^2}+\frac{1}{r^3}\left\{-\frac{3(1-2\mu)}{2(1-\mu)}\alpha_{12}\right\}\frac{\partial\psi}{\partial r}\\&+\frac{1}{r^4}\left\{\frac{1-4\mu}{2(1-\mu)}\alpha_6+\frac{3(1-2\mu)}{2(1-\mu)}\alpha_{11}\right\}\frac{\partial\psi}{\partial\theta}+\frac{1}{r^4}\left\{\frac{3(1-2\mu)}{2(1-\mu)}\alpha_{12}\right\}\psi=0\end{aligned} \tag{3b}$$

In this case, one of (3) should be eliminated reasonably for getting the solution of displacement function $\psi(r, \theta)$. In mathematical method, one of (3) should automatically satisfy the equation. Fortunately, when the coefficients of all partial derivatives of displacement function $\psi(r, \theta)$ and the coefficient of displacement function $\psi(r, \theta)$ in one of (3) are all zero, the left and right terms of this equation will be all zero and equal to each other.

If the coefficients in (3a) are all zero, equation (3b) becomes the only equation to solve the displacement function $\psi(r, \theta)$, which is called governing equation. Hence, the coefficients of all partial derivatives of displacement function $\psi(r, \theta)$ and the coefficient of displacement function $\psi(r, \theta)$ in (3a) equate to zero. The values of coefficients α_i can be obtained and substituted into (3b). The explicit expression of governing equation in the form of displacement function $\psi(r, \theta)$ is shown as follows.

$$\begin{aligned}&\frac{\partial^4\psi}{\partial r^4}+\frac{1}{r^4}\frac{\partial^4\psi}{\partial\theta^4}+\frac{2}{r^2}\frac{\partial^4\psi}{\partial r^2\partial\theta^2}-\frac{2}{r}\frac{\partial^3\psi}{\partial r^3}-\frac{6}{r^3}\frac{\partial^3\psi}{\partial r\partial\theta^2}+\\&\frac{5}{r^2}\frac{\partial^2\psi}{\partial r^2}+\frac{10}{r^4}\frac{\partial^2\psi}{\partial\theta^2}-\frac{9}{r^3}\frac{\partial\psi}{\partial r}+\frac{9}{r^4}\psi=0\end{aligned} \tag{4}$$

Equation (4) gives the expression of governing equation in plane strain problem in polar coordinates. Similarly, if (3b) automatically satisfy the equation, equation (3a) will be the only equation in the form of displacement function $\psi(r, \theta)$. The explicit expression of governing equation in the form of displacement function $\psi(r, \theta)$ is also obtained in the same way, which is the same with (4). Thus, the conclusion is that the governing equation of polar coordinates plane problem is unique.

B. Physical Components Expressed by Displacement Function

To solve (4), the boundary conditions should be provided at any point of all boundaries. Thus, it is necessary to describe physical components in the form of displacement function $\psi(r, \theta)$. There are two displacement components, including radial displacement u_r and circumferential displacement u_θ. There are three stress components, including radial stress σ_r, circumferential stress σ_θ and shear stress $\tau_{r\theta}$.

Displacement components expressed by displacement function $\psi(r, \theta)$ are shown as follows.

$$u_r=-\frac{1}{2r(1-\mu)}\frac{\partial^2\psi}{\partial r\partial\theta}+\frac{(5-4\mu)}{2r^2(1-\mu)}\frac{\partial\psi}{\partial\theta} \tag{5a}$$

$$u_\theta = \frac{\partial^2\psi}{\partial r^2} + \frac{(1-2\mu)}{2r^2(1-\mu)}\frac{\partial^2\psi}{\partial\theta^2} - \frac{3}{r}\frac{\partial\psi}{\partial r} + \frac{3}{r^2}\psi \tag{5b}$$

Stress components expressed by displacement function $\psi(r, \theta)$ are shown as follows.

$$\sigma_r = \frac{E}{2(1+\mu)}\left[-\frac{1}{r}\frac{\partial^3\psi}{\partial r^2\partial\theta} + \frac{\mu}{r^3(1-\mu)}\frac{\partial^3\psi}{\partial\theta^3} + \frac{(6-5\mu)}{r^2(1-\mu)}\frac{\partial^2\psi}{\partial r\partial\theta} - \frac{(10-9\mu)}{r^3(1-\mu)}\frac{\partial\psi}{\partial\theta}\right] \tag{6a}$$

$$\sigma_\theta = \frac{E}{2(1+\mu)}\left[\frac{(2-\mu)}{r(1-\mu)}\frac{\partial^3\psi}{\partial r^2\partial\theta} + \frac{1}{r^3}\frac{\partial^3\psi}{\partial\theta^3} - \frac{(7-5\mu)}{r^2(1-\mu)}\frac{\partial^2\psi}{\partial r\partial\theta} + \frac{(11-9\mu)}{r^3(1-\mu)}\frac{\partial\psi}{\partial\theta}\right] \tag{6b}$$

$$\tau_{r\theta} = \frac{E}{2(1+\mu)}\left[\frac{\partial^3\psi}{\partial r^3} - \frac{\mu}{r^2(1-\mu)}\frac{\partial^3\psi}{\partial r\partial\theta^2} - \frac{4}{r}\frac{\partial^2\psi}{\partial r^2} + \frac{1+\mu}{r^3(1-\mu)}\frac{\partial^2\psi}{\partial\theta^2} + \frac{9}{r^2}\frac{\partial\psi}{\partial r} - \frac{9}{r^3}\psi\right] \tag{6c}$$

III. Numerical Analysis of Stress for Circular Rock Stratum

A. Object for Investigating

The schematic diagram of coal extractions in circular rock strata is shown in Fig. 1 according to the characteristics of circular rock stratum. The shape of rock strata is simplified as an arc with a radius for the feasibility of theoretical analysis. After coal extractions, the confining stress reduces to zero on the boundary of goaf and the stress is redistributed in the overburden and floor. From the perspective of deformation, the overburden above the goaf will be collapsing and the floor below the goaf will be uplifting, which will lead to unstable deformation and affect mining production. The object for investigating is the red area in Fig. 1, that is, the first rock stratum above the goaf.

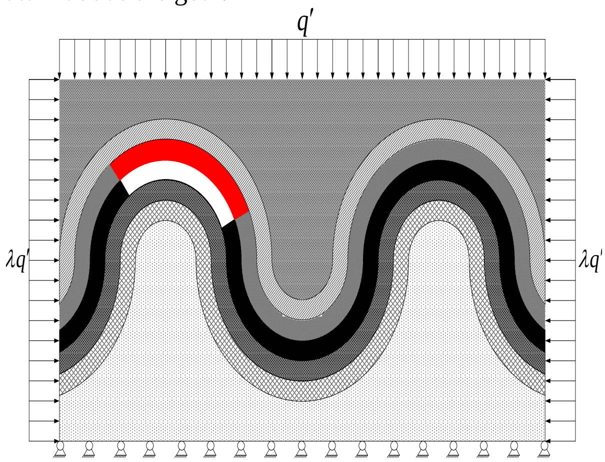

Fig. 1. Schematic diagram of coal extractions in circular rock strata

B. Numerical Modeling for Computation

The numerical modeling for computation in circular rock stratum in plane strain problem is given in Fig. 2, where r_{ib} and r_{ob} are the inner radius and outer radius, respectively.

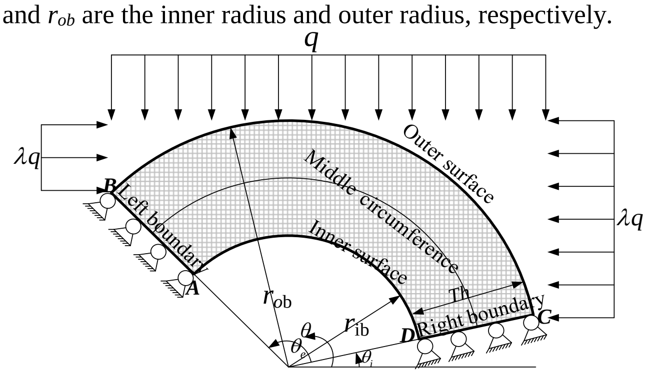

Fig. 2. Numerical modeling for computation in circular rock stratum

The conditions at left boundary or right boundary are the displacement restrain with roller support. The boundary condition in the outer surface is the stress restrain caused by horizontal stress λq and vertical stress q in rock strata (the parameter λ is the tectonic stress coefficient), while the stress in the inner surface is zero due to coal extractions. The angle θ_i between the horizontal line and right boundary is named as mining position, and the angle θ_e between left boundary and right boundary is named as advancing angle. The thickness of circular rock stratum is marked as "*st*".

In this paper, the finite difference method is used to solve the displacement function $\psi(r, \theta)$, and there are many finite discrete points in the computation domain. The discrete points in the computation domain should satisfy the governing equation (4) and the discrete points at the boundary should satisfy boundary conditions in Fig. 2. Table I lists the values of stress and displacement at the all boundaries, and Table II lists the values of stress and displacement at the four corner points in numerical modeling. It is obvious that three out of four conditions should be satisfied at each corner point, which is superior to the traditional computing method with only two out of four conditions being satisfied. Therefore, the stress solutions around the corner region obtained by this method will be closer to the actual state, while these values obtained by traditional method will deviate from the actual state. The mesh length in radial and circumferential direction is 0.5m and 1°, respectively.

Table I
Boundary Conditions

Boundary	Boundary Conditions: Normal Component	Boundary Conditions: Tangential Component
right boundary $\theta = \theta_i$	$u_r(r,\theta_i) = 0$	$u_\theta(r,\theta_i) = 0$
left boundary $\theta = \theta_{\max} = \theta_i + \theta_e$	$u_r(r,\theta_{\max}) = 0$	$u_\theta(r,\theta_{\max}) = 0$
inner surface $r = r_{ib}$	$\sigma_r(r_{ib},\theta) = 0$	$\tau_{r\theta}(r_{ib},\theta) = 0$
outer surface $r = r_{ob}, \theta \le 90^\circ$	$\sigma_r(r_{ob},\theta) = -q(\lambda\cos\theta + \sin\theta)$	$\tau_{r\theta}(r_{ob},\theta) = -q(\cos\theta - \lambda\sin\theta)$
outer surface $r = r_{ob}, \theta > 90^\circ$	$\sigma_r(r_{ob},\theta) = -q(-\lambda\cos\theta + \sin\theta)$	$\tau_{r\theta}(r_{ob},\theta) = -q(\cos\theta + \lambda\sin\theta)$

Table II
Boundary Conditions at the Four Corner Points

Corner Point	Boundary Conditions	Given Boundary Conditions
A	$\{u_r, u_\theta, \sigma_r, \tau_{r\theta}\}$	$u_r = 0; u_\theta = 0; \tau_{r\theta} = 0$
B	$\{u_r, u_\theta, \sigma_r, \tau_{r\theta}\}$	$u_r = 0; u_\theta = 0; \tau_{r\theta} = 0$
C	$\{u_r, u_\theta, \sigma_r, \tau_{r\theta}\}$	$u_r = 0; u_\theta = 0; \tau_{r\theta} = 0$
D	$\{u_r, u_\theta, \sigma_r, \tau_{r\theta}\}$	$u_r = 0; u_\theta = 0; \tau_{r\theta} = 0$

C. Stress Distribution

a: The Factor of Inner Radius

Given that the tectonic stress coefficient λ is 1.8, the mining depth *md* is 1000m, the mining position θ_i is 0°, the advancing angle θ_e is 120°, the thickness of circular rock stratum *st* is 20m and the inner radius r_{ib} is assigned as 5m, 10m, 20m, 40m, 50m, 60m, 80m and 100m, respectively, the stress components along middle circumference with different inner radii are presented as follows.

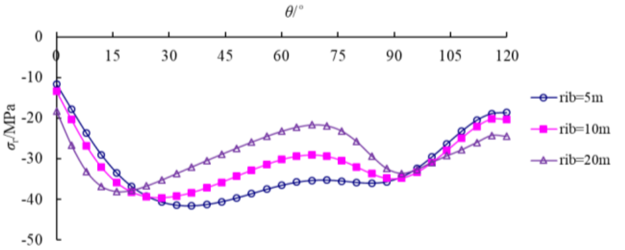

(a)

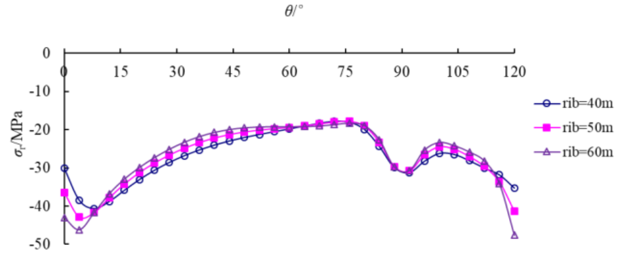

(b)

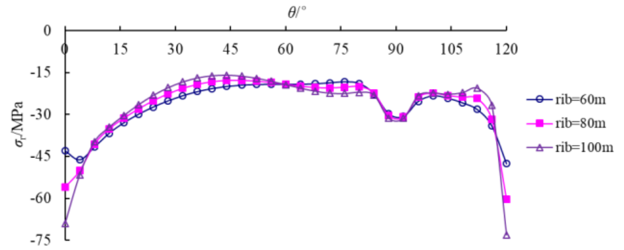

(c)

Fig. 3. The radial stress distribution along middle circumference with different inner radii

Fig. 3 shows the radial stress distribution along middle circumference with different inner radii. The results show that the radial stress at left boundary or right boundary increases gradually with the increasing of inner radius. For instance, the radial stresses at left boundary and right boundary increase from 18.65MPa and 11.60MPa to 73.05MPa and 69.08MPa when the inner radius increases from 5m to 100m. The radial stress increases by nearly 3 ~ 5 times at left boundary or right boundary when the inner radius increases by 19 times, that is, from 5m to 100m. It can be obtained that the growth rate of radial stress is much smaller than that of inner radius. It should be noted that the peak value of radial stress along middle circumference does not always increase with the increasing of inner radius. The peak value of radius stress decreases from 41.61MPa to 38.14MPa when the inner radius increases from 5m to 20m, and it increases from 40.61MPa to 69.08MPa when the inner radius increases from 40m to 100m. Meanwhile, the position of peak value of radius stress varies with different inner radii. For example, the position of peak value of radial stress is located from θ=35 ° to θ=0 ° when the inner radius increases from 5m to 100m. Therefore, it can be concluded that the peak value of radius stress will move toward the right boundary with the increasing of inner radius.

It can be seen from Fig. 4 that the circumferential stress distribution curves with different inner radii are basically the same. With the increasing of inner radius, the value of circumferential stress increases gradually, and so does the peak value of circumferential stress. An example shows that the peak value of circumferential stress increases from 60.99MPa to 329.94MPa when the inner radius increases from 5m to 100m. The circumferential stress increases by about 4 times when the inner radius increases by 19 times. Obviously, the growth rate of circumferential stress is much smaller than that of inner radius. It should be worth noting that the position of peak value of circumferential stress is around at θ=90 ° for all inner radii except the inner radius being 5m. The position of peak value of circumferential stress is easy to cause circumferential compression failure in circular rock stratum. Therefore, more observation should be made and more measures should be taken around the location of θ=90 ° for avoiding the disastrous accidents during the coal mining advancing in circular rock stratum.

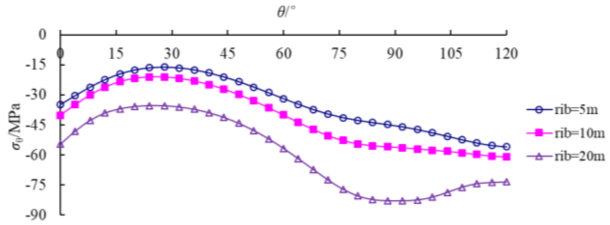

(a)

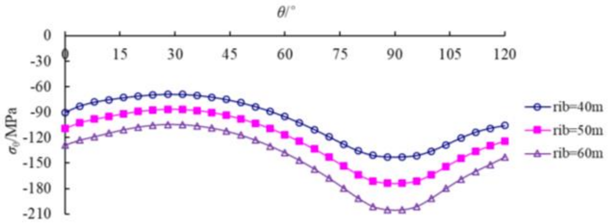

(b)

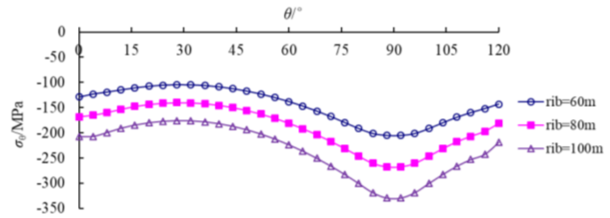

(c)

Fig. 4. The circumferential stress distribution along middle circumference with different inner radii

The peak value of shear stress basically increases with the increasing of inner radius in Fig. 5. For example, the peak value of shear stress increases from 23.97MPa to 97.65MPa when the inner radius increases from 5m to 100m. The shear stress increases by about 3 times when the inner radius increases by 19 times. Obviously, the growth rate of shear stress is also much smaller than that of inner radius. It is noteworthy that the shear stress at right boundary increases from 22.75MPa to 42.29MPa when the inner radius increases from 5m to 40m, but it is stable at about 43MPa when the inner radius increases from 40m to 100m. However, the shear stress at left boundary is increasing with the increasing of inner radius when the inner radius exceeds 40m. Thus, it can be concluded that the effect of inner radius on shear stress is not significant for right boundary while the effect is significant for left boundary. The results also show that the position of peak value of shear stress is stable within the range of θ=5 ° ~6 ° under different inner radii, indicating that the effect of inner radius on the position of peak value of shear stress is not significant.

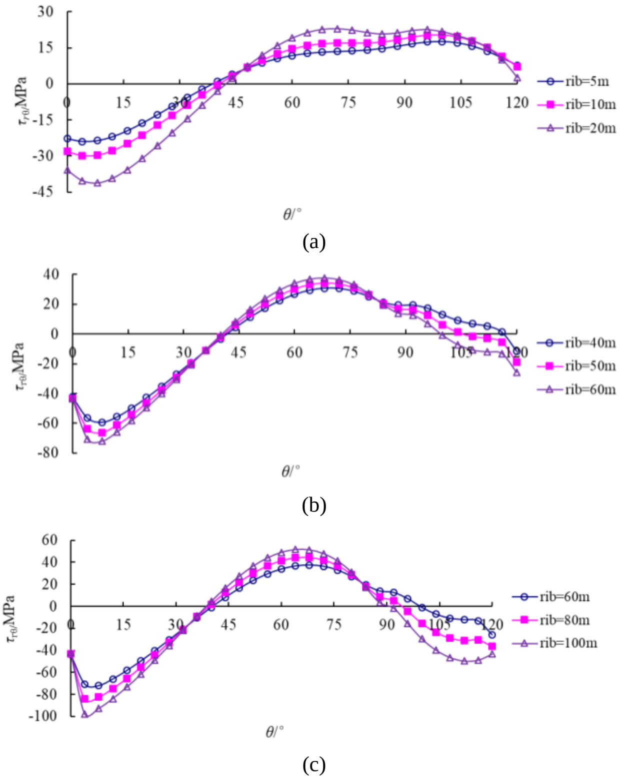

Fig. 5. The shear stress distribution along middle circumference with different inner radii

b: The Factor of Tectonic Stress Coefficient

Given that the inner radius r_{ib} is 20m, the mining depth *md* is 1000m, the mining position θ_i is 0°, the advancing angle θ_e is 120°, the thickness of circular rock stratum *st* is 20m and the tectonic stress coefficient λ is assigned as 1.2, 1.5, 1.8, 2.1 and 2.4, respectively, the stress components along middle circumference with different tectonic stress coefficients are presented as follows.

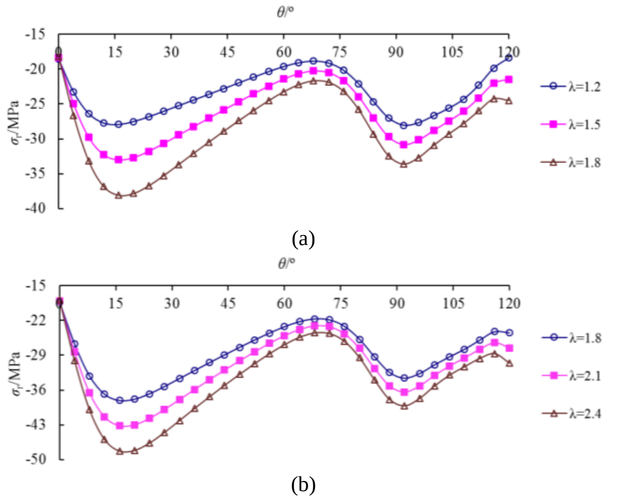

Fig. 6. The distribution of radial stress along middle circumference with different tectonic stress coefficients

According to Fig. 6, the curves of radial stress distribution are basically the same with different tectonic stress coefficients. The value of radial stress increases gradually with the increasing of tectonic stress coefficient, so does the peak value of radial stress. For example, the peak value of radial stress increases from 27.95MPa to 48.42MPa when the tectonic stress coefficient increases from 1.2 to 2.4. The radial stress increases by about 66% while the tectonic stress coefficient increases by 100%. Hence, the growth rate of radial stress is less than that of tectonic stress coefficient. Moreover, the position of peak value of radial stress changes from $\theta=15°$ to $\theta=18°$ with the increasing of tectonic stress coefficient. It can be concluded that the position of peak value of radial stress will move toward the left boundary with the increasing of tectonic stress coefficient, but not significantly.

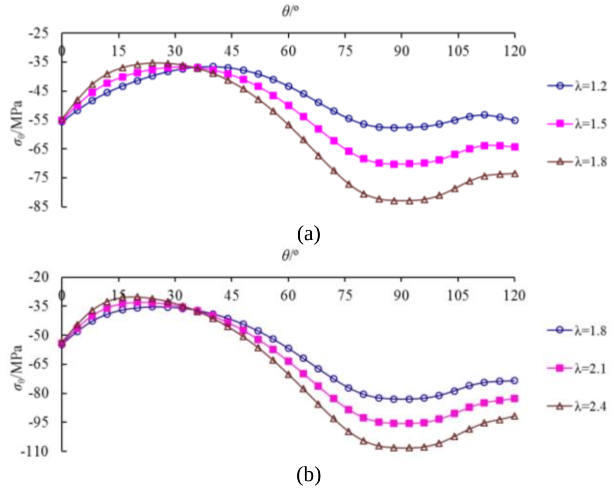

Fig. 7. The circumferential stress distribution along middle circumference with different tectonic stress coefficients

The effect of tectonic stress coefficient on circumferential stress is different for different cross sections according to the curves in Fig. 7. The circumferential stress in cross sections (θ=0°~34°) decreases while the circumferential stress in cross sections (θ=34°~120°) increases with the increasing of tectonic stress coefficient. For instance, the circumferential stress at right boundary (θ=0°) decreases from 55.67MPa to 53.59MPa when the tectonic stress coefficient increases from 1.2 to 2.4, while the circumferential stress at left boundary (θ=120°) increases from 55.19MPa to 91.79MPa. It can be concluded that the circumferential stress around right boundary decreases with the increasing of tectonic stress coefficient, whereas the circumferential stress far away from right boundary increases. At the same time, the position of peak value of circumferential stress is also slightly different with the increasing of tectonic stress coefficient. The position of peak value changes from θ=88° to θ=91° when the tectonic stress coefficient increases from 1.2 to 2.4. It can be a conclusion that the peak value of circumferential stress moves toward left boundary, but not significantly. Therefore, more observation should be made and more measures should be taken around the location of θ=90° for avoiding disastrous accidents during the coal mining advancing in circular rock stratum.

The effect of tectonic stress coefficient on shear stress is either not the same for different cross sections according to the curves in Fig. 8. The shear stress in cross sections (θ=0°~30° and θ=45°~105°) increases with the increasing of tectonic stress coefficient, but the shear stress in other cross sections decreases with the increasing of tectonic stress coefficient. For example, the shear stress at right boundary (θ=0°) increases from 21.53MPa to 50.15MPa, while the shear stress at left boundary (θ=120°) decreases from 9.85MPa to -4.39MPa when the tectonic stress coefficient increases from 1.2 to 2.4. It indicates that the shear stress around right boundary increases with the increasing of tectonic stress coefficient, while the shear stress far away from right boundary decreases. Meanwhile, the position of peak value changes from θ=11° to θ=7° when the tectonic stress coefficient increases from 1.2 to 2.4. This result suggests that the position of peak value of shear stress moves toward right boundary, but not obviously.

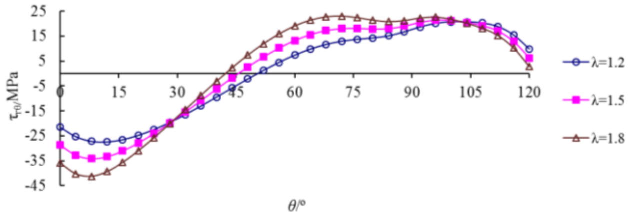

(a)

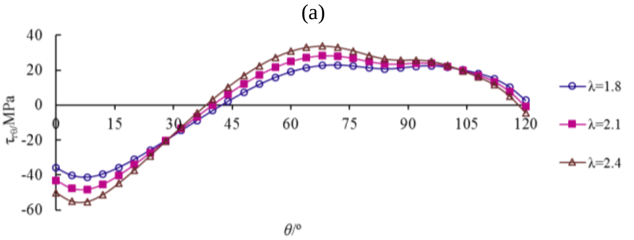

(b)

Fig. 8. The shear stress distribution along middle circumference with different tectonic stress coefficients

c: The Factor of Mining Depth

Given that the inner radius r_{ib} is 20m, the tectonic stress coefficient λ is 1.8, the mining position θ_i is 0°, the advancing angle θ_e is 120°, the thickness of circular rock stratum *st* is 20m, and the mining depth *md* is assigned as 600m, 800m, 1000m, 1200m, and 1400m, respectively, the stress components along middle circumference with different mining depths are presented as follows.

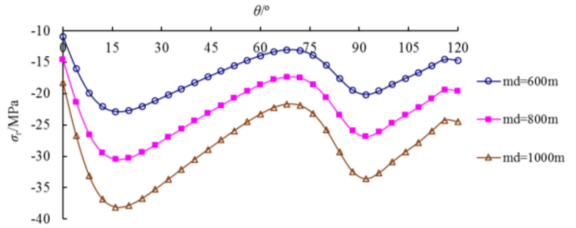

(a)

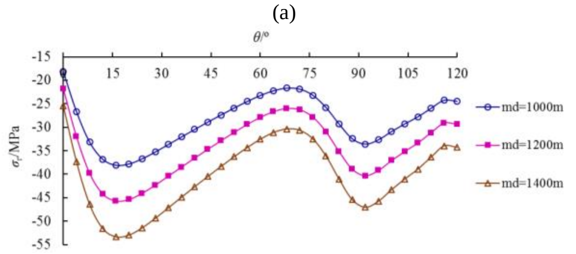

(b)

Fig. 9. The radial stress distribution along middle circumference with different mining depths

According to Fig. 9, the curves of radial stress distribution are basically the same with different mining depths. The value of radial stress increases gradually with the increasing of mining depth, so does the peak value of radial stress. For instance, the peak value of radial stress increases from 22.88MPa to 53.39MPa when the mining depth increases from 600m to 1400m. The radial stress increases by 1.33 times when the mining depth increases by 1.33 times as well. In fact, the radial stress for all cross sections increases by 1.33 times with the mining depth increasing by 1.33 times as well. Therefore, the radial stress is linear with the mining depth. Meanwhile, regardless of the mining depth, the position of peak value of radial stress remains in the same cross section with θ=17°. It can be concluded that the mining depth will not change the position of peak value of radial stress.

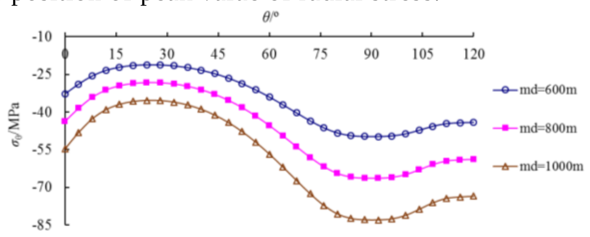

(a)

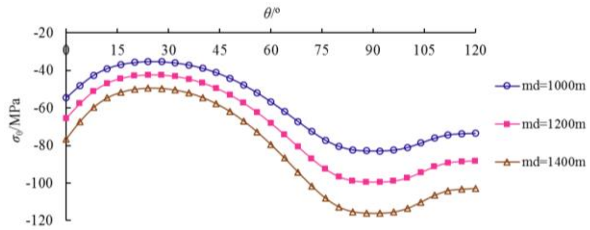

(b)

Fig. 10. The circumferential stress distribution along middle circumference with different mining depths

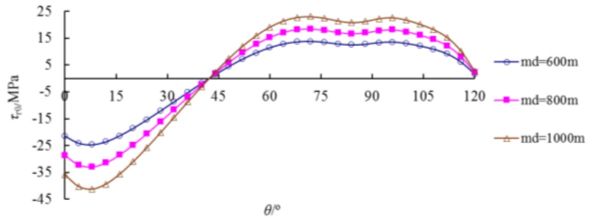

(a)

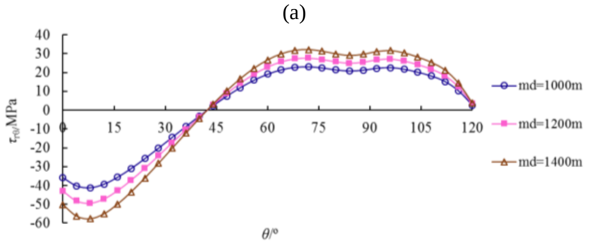

(b)

Fig. 11. The shear stress distribution along middle circumference with different mining depths

From Fig. 10 and Fig. 11, the effect of mining depth on circumferential stress or shear stress is the same as that of mining depth on radial stress. There is also a linear relationship between the circumferential stress and the mining depth, or, between the shear stress and the mining depth. Moreover, the mining depth will not change the position of peak value of circumferential stress or shear stress.

d: The Factor of Advancing Angle

Given that the inner radius r_{ib} is 20m, the tectonic stress coefficient λ is 1.8, the mining depth *md* is 1000m, the mining position θ_i is 0°, the thickness of circular rock stratum *st* is

20m, and the advancing angle θ_e is assigned as 30°, 60°, 90°, 120°, 150° and 180°, respectively, the stress components along middle circumference with different advancing angles are presented as follows.

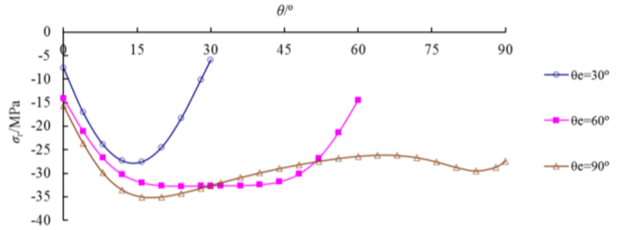

(a)

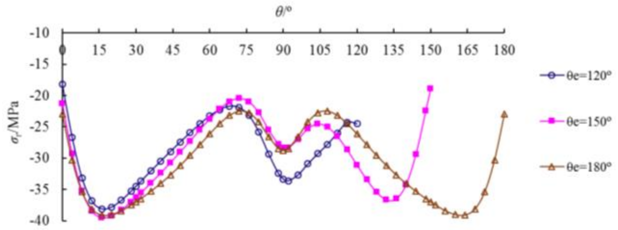

(b)

Fig. 12. The radial stress distribution along middle circumference with different advancing angles

As can be seen from Fig. 12, the distribution of radial stress varies with different advancing angles. The radial stress first increases and then decreases along circumferential direction when the advancing angle is less than 90°, while the radial stress increases and decreases alternately along circumferential direction when the advancing angle is greater than 90°. In particular, when the advancing angle is equal to 180°, the radial stress distribution is symmetrical when the loading and constraint in numerical modeling are symmetrical. The peak value of radial stress increases with the increasing of advancing angle. For example, the peak value of radial stress increases from 27.86MPa to 39.14MPa when the advancing angle increases from 30° to 180°. Obviously, the advancing angle increases by 5 times while the peak value of radial stress increases by only 40%. Therefore, the growth rate of radial stress is much smaller than that of advancing angle. Besides, the position of peak value of radial stress is far away from right boundary with the increasing of advancing angle, and then tends to be stable in the cross section with θ=17°.

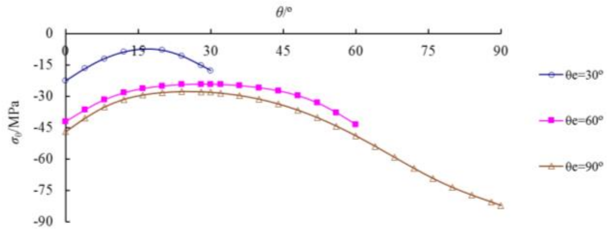

(a)

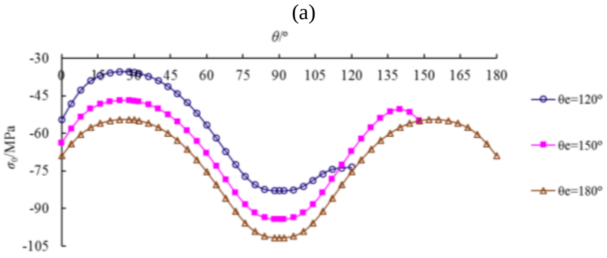

(b)

Fig. 13. The circumferential stress distribution along middle circumference with different advancing angles

The variations of circumferential stress are not the same with different advancing angles as shown in Fig. 13. For example, the circumferential stress first decreases and then increases along circumferential direction when the advancing angle is less than 90°, while it decreases and increases alternately when the advancing angle is greater than 120°. Similar to radial stress, the distribution of circumferential stress is also symmetrical when the advancing angle is equal to 180°. The value of circumferential stress increases gradually with the increasing of advancing angle, as well as the peak value of circumferential stress. For example, the peak value of circumferential stress increases from 22.61MPa to 101.62MPa when the advancing angle increases from 30° to 180°. The advancing angle increases by 5 times while the peak value of circumferential stress increases by 3.5 times. Thus, the advancing angle not only affects the distribution of circumferential stress, but also significantly affects the value of circumferential stress. Meanwhile, the position of peak value of circumferential stress varies with the increasing of advancing angle. The peak value of circumferential stress is at right boundary while the advancing angle is less than 60°, but it is located in the cross section with θ=90° when the advancing angle is greater than 60°. Therefore, more observation should be made and more measures should be taken at right boundary when the advancing angle is less than 60°, while more observation should be made and more measures should be taken in the cross section with θ=90° when the advancing angle is greater than 60°.

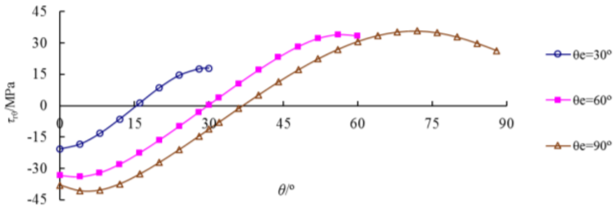

(a)

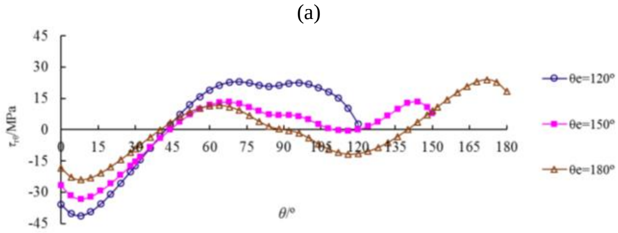

(b)

Fig. 14. The shear stress distribution along middle circumference with different advancing angles

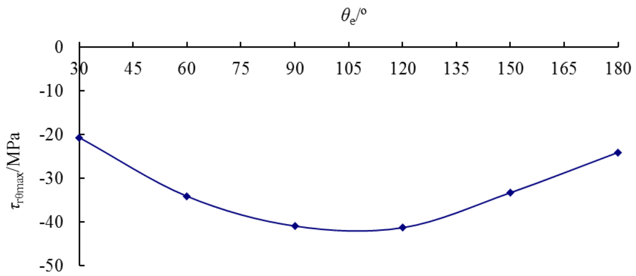

Fig. 15. The relationship between peak value of shear stress and advancing angle

According to Fig. 14, the shear stress increases and decreases alternately along circumferential direction, especially for large values of advancing angle. Contrary to radial stress and circumferential stress, the distribution of shear stress is anti-symmetrical when the advancing angle is equal to 180°. Fig. 15 shows the relationship between peak value of shear stress and advancing angle. As can be seen from Fig. 15, the peak value of shear stress first increases and then decreases with the increasing of advancing angle. At the same time, the position of peak value of shear stress changes from θ=0° to θ=8° when the advancing angle increases from 30° to 180°. The conclusion is that the position of peak value of shear stress tends to be far away from right boundary, but not significantly.

e: The Factor of Mining Position

This part analyzes the cross sections with the same angle from right boundary for different mining positions in numerical modeling, which is defined as θ-θ_i. Given that the inner radius r_{ib} is 20m, the tectonic stress coefficient λ is 1.8, the mining depth *md* is 1000m, the advancing angle θ_e is 120°, the thickness of circular rock stratum *st* is 20m and the mining position θ_i is assigned as 0°, 15°, 30°, 45° and 60°, respectively, the stress components along middle circumference in different mining positions are presented as follows.

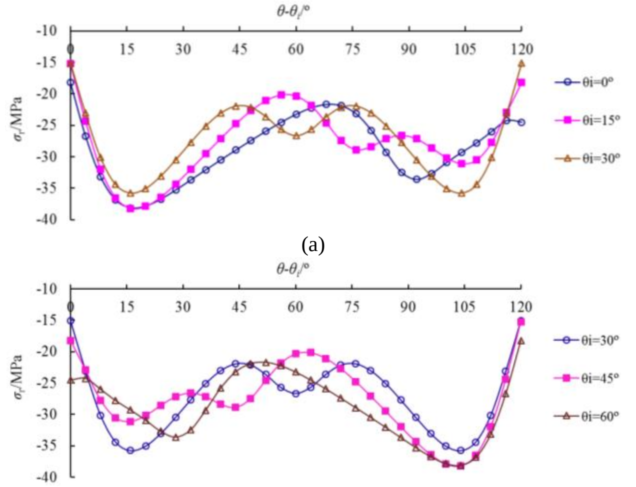

Fig. 16. The radial stress distribution along middle circumference with different mining positions

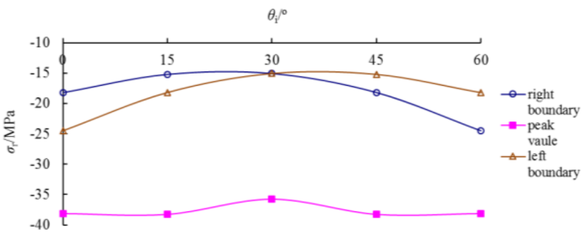

Fig. 17. The variation of radial stress with different mining positions

According to Fig. 16, the radial stress increases and decreases alternately along circumferential direction. Here, the radial stress at right boundary, left boundary and the peak value of radial stress are mainly analyzed, which is shown in Fig. 17. The results show that the radial stresses in these cross sections decrease first and then increase with the increasing of mining position. Obviously, a minimum value of radial stress exists nearby the mining position at the angle of 30°. In fact, the distribution of radial stress is symmetrical under the loading and restrain in numerical modeling when the mining position is at the angle of 30°. Therefore, the right boundary should be located around the angle of 30° for coal mining in circular rock stratum. It should be noted that there are two equal peak values of radial stress when the mining location is at the angle of 30°. The position of peak value is close to the right boundary when the mining position is smaller than 30°, while it is close to left boundary when the mining position is larger than 30°.

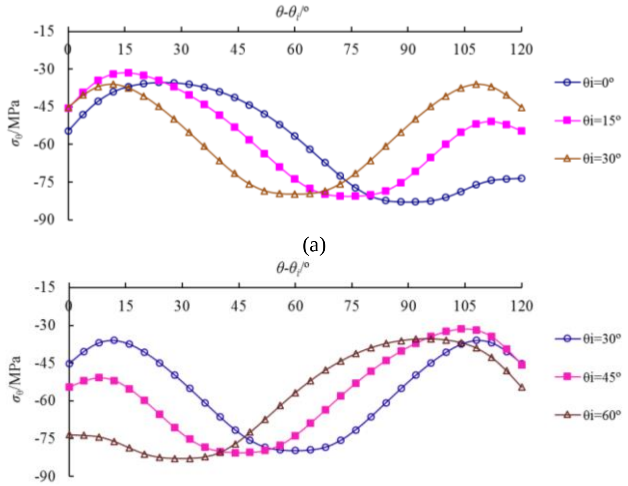

Fig. 18. The circumferential stress distribution along middle circumference with different mining positions

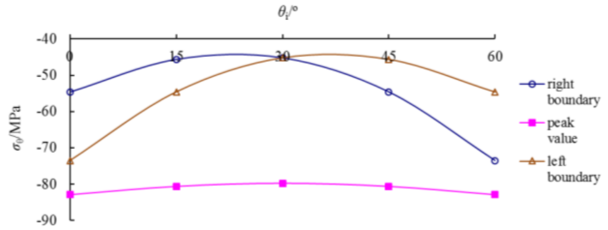

Fig. 19. The variation of circumferential stress with different mining positions

The circumferential stress decreases and increases alternately along circumferential direction as shown in Fig. 18. Still, the circumferential stress at right boundary, left boundary and the peak value of circumferential stress are mainly analyzed in Fig. 19. The results show that the circumferential stress in these cross sections first decreases and then increases with the increasing of mining position. A minimum value of circumferential stress exists nearby the mining position at the angle of 30° as well as the characteristic of radial stress. It should be noted that the peak value of circumferential stress is located at the highest point of numerical modeling for different mining positions. For example, the peak value of circumferential stress is located at the angle of 75° from right boundary when the mining position is equal to 15°, which is the highest point in numerical modeling. Therefore, more observation should be made and more measures should be taken at the anticline ridge in circular rock stratum during the mining advancing.

The shear stress decreases and increases alternately along circumferential direction as shown in Fig. 20. Obviously, the shear stress has negative and positive values. Similarly, the shear stress at right boundary, left boundary and the peak value of shear stress are mainly analyzed in Fig. 21. The positive peak values of shear stress increase while the negative peak values decrease with the increasing of mining position. The feasible position for right boundary is at the angle of 30 °in circular rock stratum. On the other hand, the variation of the position of positive peak value is just the opposite to that of negative peak value. Therefore, the mining position has significant effect on the position of peak value of shear stress.

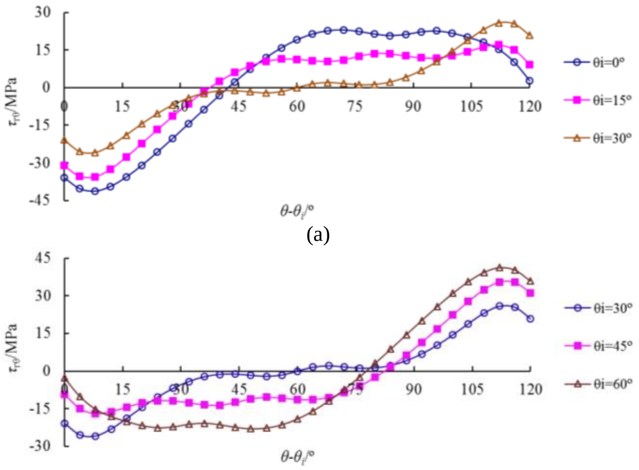

(a)

(b)

Fig. 20. The shear stress distribution along middle circumference with different mining positions

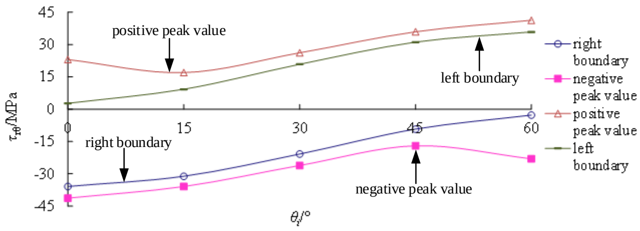

Fig. 21. The variation of shear stress with different mining positions

f: The Factor of Thickness of Circular Rock Stratum

Given that the inner radius r_{ib} is 20m, the tectonic stress coefficient λ is 1.8, the mining depth *md* is 1000m, the advancing angle θ_e is 120 °, the mining position θ_i is 0 °and the thickness of circular rock stratum *st* is assigned as 10m, 15m, 20m, 25m and 30m, respectively, the stress components along middle circumference with different thicknesses of circular rock stratum are presented as follows.

Fig. 22 shows the radial stress increasing and decreasing alternately along circumferential direction. The radial stress increases with the increasing of thickness of circular rock stratum in some cross sections, while it decreases in other cross sections. Fig. 23 shows the radial stress distribution with different thicknesses of circular rock stratum in four cross sections (θ=0 °, 30 °,90 °,120 °). It can be seen that the radial stress at right boundary (θ=0 °) or left boundary (θ=120 °) decreases with the increasing of thickness of circular rock stratum, but the radial stress in cross sections (θ=30 °and 90 °) increases. Clearly, the radial stress in cross sections within the range of 30 ° ~ 90 ° increases with the increasing of thickness of circular rock stratum. Fig. 24 shows the variation of peak value of radial stress with different thicknesses of circular rock stratum. Obviously, the peak value of radial stress first decreases and then increases with the increasing of thickness of circular rock stratum. A minimum value of radial stress exists when the thickness of circular rock stratum is 20m. In addition, the position of peak value of radial stress moves toward left boundary with the increasing of thickness of circular rock stratum, but not significantly. For example, the position of peak value of radial stress changes from θ=8 ° to θ=23 ° when the thickness of circular rock stratum increases from 10m to 30m.

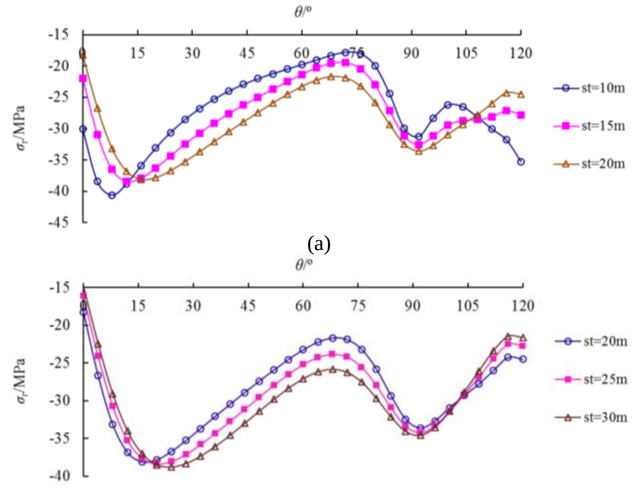

(a)

(b)

Fig. 22. The radial stress distribution along middle circumference with different thicknesses of circular rock stratum

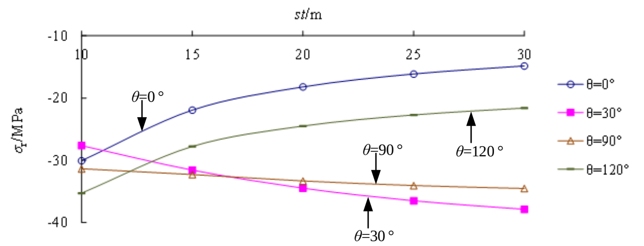

Fig. 23. The radial stress distribution with different thicknesses of circular rock stratum in four cross sections

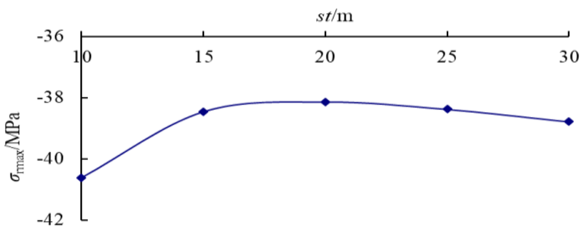

Fig. 24. The variation of peak value of radial stress with different thicknesses of circular rock stratum

Fig. 25 shows the variation of circumferential stress with different thicknesses of circular rock stratum. Obviously, the circumferential stress decreases and increases alternately along circumferential direction. The peak value of circumferential stress decreases with the increasing of thickness of circular rock stratum. For instance, the peak value of circumferential stress decreases from 142.85MPa to 64.83MPa when the thickness of circular rock stratum increases from 10m to 30m. Meanwhile, the position of peak value of circumferential stress changes from 90 °to 97 °when the thickness of circular rock stratum increases from 10m to 30m. It can be concluded that the increasing of thickness of circular rock stratum makes the position of peak value of circumferential stress move toward the left boundary, but not significantly. Therefore, the increasing of thickness of circular rock stratum plays a positive role in reducing the circumferential stress, and the position of peak value of circumferential stress is always around the angle of 90 °. More observation should be made and more measures should be taken at the location of θ=90 ° for avoiding disastrous accidents during the mining advancing in circular rock stratum.

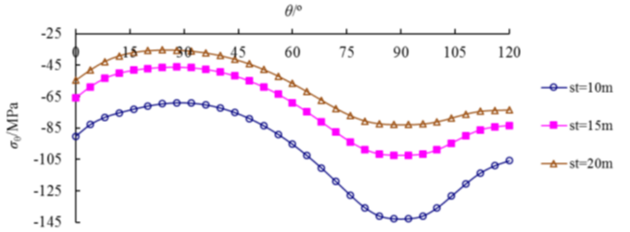

(a)

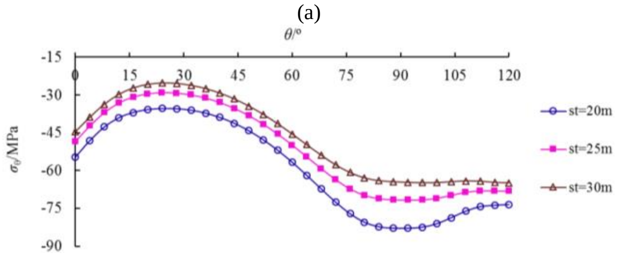

(b)

Fig. 25. The circumferential stress distribution along middle circumference with different thicknesses of circular rock stratum

Fig.26 shows that the shear stress increasing and decreasing alternately along circumferential direction. The shear stress within the range of 0 °~90 ° decreases with the increasing of thickness of circular rock stratum, so does the peak value of shear stress, but it decreases within the range of 90 °~120 °. For example, the peak value of shear stress decreases from 59.43MPa to 33.85MPa when the thickness of circular rock stratum increases from 10m to 30m. In addition, the position of peak value of shear stress is basically stable within the range of 6 °~7 °. Therefore, it can be concluded that the thickness of circular rock stratum plays a positive role in reducing the value of shear stress, but has no significant effect on the position of peak value of shear stress.

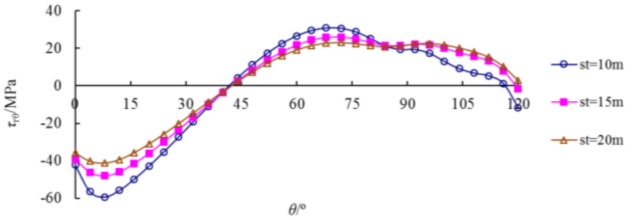

(a)

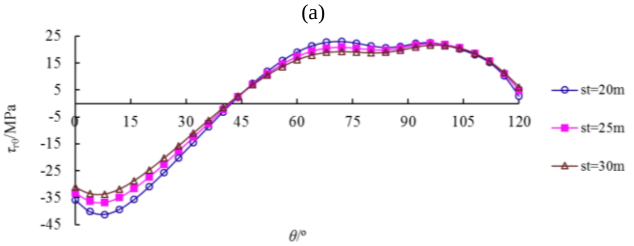

(b)

Fig. 26. The shear stress distribution along middle circumference with different thicknesses of circular rock stratum

IV. Field Application in Fold Structure

A. *Geological Conditions*

No. 2502 mining area is located at the depth of + 860m ~ + 1200m in China. The thickness of coal seam is within the range of 18.2m~54.5m and its average thickness is about 31m. The geological conditions in this mining project are more complicated because of the geological structure, especially the fold structure. The syncline and anticline are alternately distributed from north to south with a distance of 2600m in this mining project. Full-mechanized caving mining method is used for coal extractions along the fold structure of syncline and anticline. Fig. 27 shows the part of geological sections in this mining project.

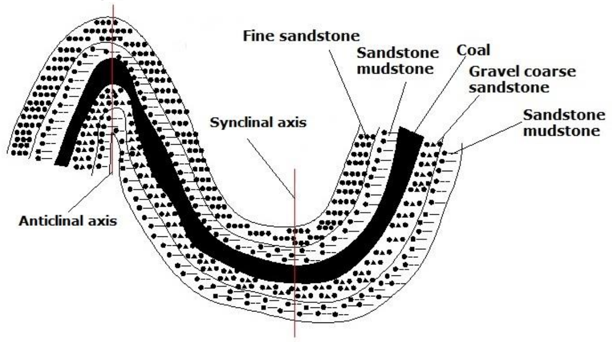

Fig. 27. The part of geological section

B. *Numerical Modeling for a Circular Arc-shaped Fold Structure*

The schematic diagram of coal extractions is established as shown in Fig. 28 based on the geological conditions in No.2502 mining area. Here, the fold structure is simplified to arc shape, which is similar to that in section III. The open-off cut is located at the groove point of syncline, and the working face is pushed up to the ridge point of anticline. The research object is the first overburden above the goaf, that is, the red area in Fig. 28. Fig. 29 shows the numerical modeling in plane strain problem, and the boundary conditions of displacement or stress. The mining depth is assigned as 1000m, the thickness of rock stratum is assigned as 16.8m, and the tectonic stress coefficient λ is assigned as 2. The radius of rock stratum at lower boundary in syncline is 56.8m, and the radius of rock stratum at lower boundary in anticline is 40m. The mesh length in radial and circumferential direction is 0.4m and 1 °, respectively. The physical and mechanical parameters of rock stratum are shown in Table III.

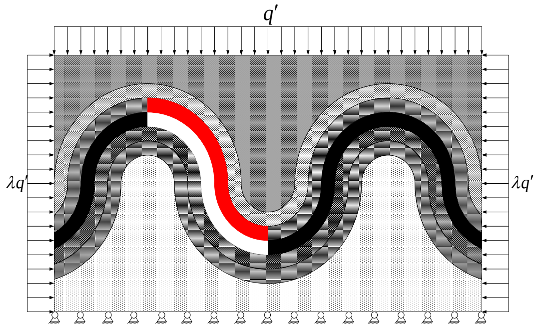

Fig. 28. Schematic diagram of coal extractions in No.2502 mining area

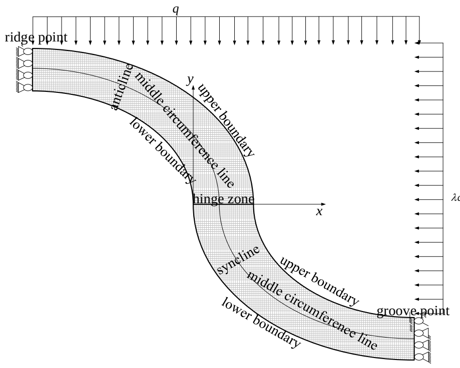

Fig. 29. Numerical modeling of coal extractions from syncline to anticline

Table III
PHYSICAL AND MECHANICAL PARAMETERS OF ROCK STRATUM

Young's Modulus	Poisson's Ratio	Density
18×10^9 Pa	0.185	2400 kg/m^{-3}

C. Stress Analysis for Circular Rock Stratum

This section analyzes the stress components when the working face is pushed upward to 30m, 60m, 90m, 110m, 130m and 150m, respectively. For feasible analysis, the coordinate transformation method is used to convert the numerical calculation results from polar coordinate system into Cartesian coordinate system. The distribution of horizontal stress σ_x, vertical stress σ_y, and shear stress τ_{xy} are shown in Figs. 30-32.

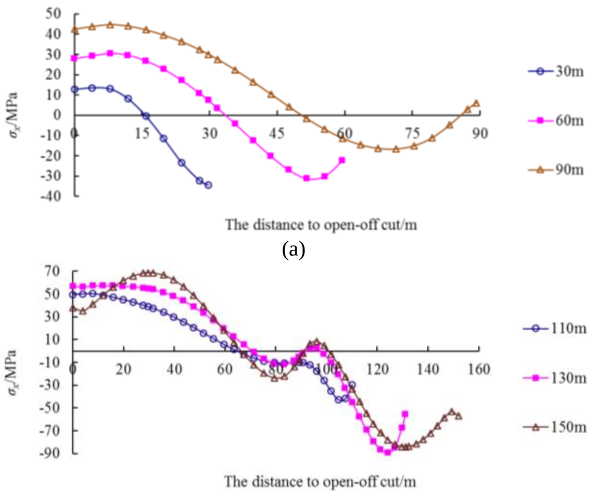

Fig. 30. The horizontal stress distribution along middle circumference with different advancing distances

As can be seen from Fig. 30, the horizontal stress along middle circumference is unevenly distributed along the upward direction and changes alternately between decreasing and increasing. Due to different advancing distances, half of the horizontal stress is tensile stress and the other half is compressive stress. The tensile stress is mainly distributed in the rock stratum in front of the open-off cut, and the compressive stress is mainly distributed in the rock stratum behind the working face. The maximum value of horizontal tensile stress is about 1.43 times than that of initial stress in rock stratum in front of open-off cut, which is easy to cause tensile fracture for rock stratum. Besides, the maximum value of horizontal compressive stress is about 1.75 times than that of initial stress in rock stratum behind working face, resulting in compression failure for rock stratum. These conclusions are basically consistent with the actual break failure of fold structure in No.2502 mining area.

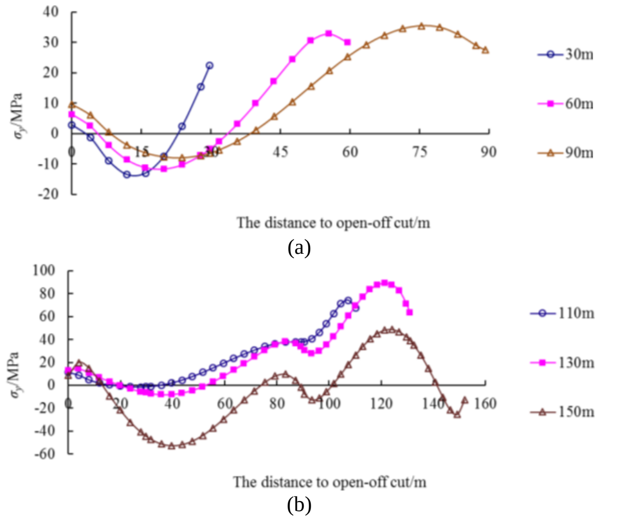

Fig. 31. The vertical stress distribution along middle circumference with different advancing distances

As shown in Fig. 31, the vertical stress along middle circumference shows an alternating variation between increasing and decreasing, which is mainly tensile stress with different advancing distances. The maximum value of vertical tensile stress is mainly distributed in the rock stratum behind working face, and is about 3.71 times than that of initial stress, which is easy to cause tensile failure for rock stratum. What's more, the vertical tensile stress at the ridge point is relatively reduced when the advancing distance is equal to 150m. These results show that, the vertical tensile stress is relatively large before working face reaching the ridge point, and it decreases when working face reaches or passes through the ridge point. Thus, working face should quickly pass through the ridge point of anticline during coal extractions for avoiding rock break failure under the condition of vertical tensile stress.

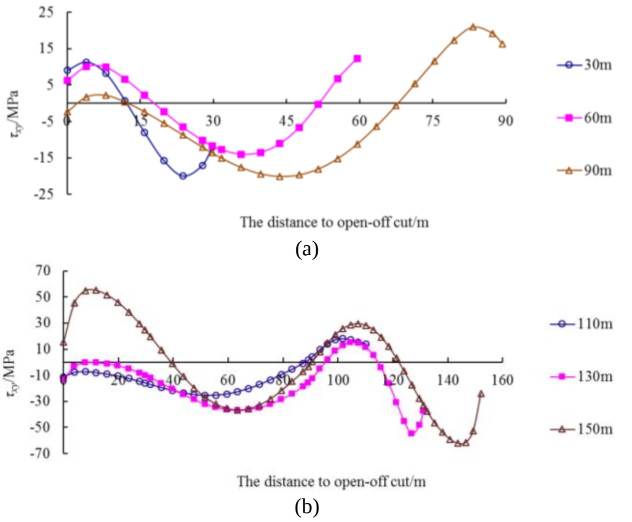

Fig. 32. The shear stress distribution along middle circumference with different advancing distances

It can be seen that the shear stress along middle circumference is unevenly distributed along the upward direction and alternates between increasing and decreasing according to Fig. 32. The maximum value of shear stress is mainly distributed in the rock stratum behind working face with different advancing distances. Thus, there might be shear damage or shear failure in the rock stratum behind working face during the process of coal extractions.

V. Conclusions

A displacement function is given in polar coordinates to solve two partial differential equations with mixed boundary conditions in elastic, isotropic and homogeneous rock. Subsequently, the displacement function is governed by a fourth-order elliptic partial differential equilibrium equation, and its numerical solution is obtained by finite difference calculation. This paper analyzes the variation of stress distribution with different influencing factors according to the analytical expressions of stress components in the form of displacement function, which is better our understanding of the stability of circular rock stratum after coal extractions. Finally, this semi-analytical elastic stress solution is applied to the fold structure in No.2502 mining area, and the dangerous positions are pointed out during the process of coal extractions, which is of enormous significance for coal mining engineering.

References

[1] W.Y. Hu, M.C. He, *The present situation and development trend for deep coal resources and the development of geological conditions*. Beijing: Coal Industry Publishing House, 2008, pp. 15-28.
[2] M.C. He, Q.H. Qian, *Mechanical foundation for deep rock mass*. Beijing: Science Press, 2010, pp. 26-46.
[3] S. P. Timoshenko, J. N. Goodier, *Theory of Elasticity*. New York: McGraw-Hill Book Company, 1979, pp. 8-15.
[4] J. T. Oden, E. A. Ripperger, *Mechanics of Elastic Structures*. New York: McGraw-Hill Book Company, 1981, pp. 10-25.
[5] R. B. Chianese, R. J. Erdlac, "The general solution to the distribution of stresses in a circular ring compressed by two forces acting along a diameter," *Quart. J. Mech. Appl. Math.*, vol. 41, no. 2, pp. 239-247, May 1988.
[6] C. Bagci, "A new unified strength of materials solution for stresses in curved beams and rings," *ASME J. Mech. Des.*, vol. 114, no. 2, pp. 231-237, Jun. 1992.
[7] C. Bagci, "Exact elasticity solutions for stresses and deflections in curved beams and rings of exponential and T-sections," *ASME J. Mech. Des.*, vol. 115, no.3, pp.346-358, Sep. 1993.
[8] R. D. Cook, "Circumferential stress in curved beams," *ASME J .Appl. Mech.*, vol. 59, no. 1, pp. 224-225, Mar. 1992.
[9] N. Tutuncu, "Plane stress analysis of end loaded orthotropic curved beams of constant thickness with applications to full rings," *ASME J. Mech. Des.*, vol. 120, no. 2, pp. 368-374, Jun. 1998.
[10] A. Sloboda, P. Honarmandi, "Generalized elasticity method for curved beam stress analysis: analytical and numerical comparison for a lifting hook," *Mech. Based Des. Struct. Mach.*, vol. 35, no. 3, pp. 319-332, Jul. 2007.
[11] A. J. Durelli, B. Ranganayakamma, "Parametric solution of stresses in beams," *J. Eng. Mech.*, vol. 115, no. 2, pp. 401-415, Feb. 1989.
[12] S. R. Ahmed, A. B. M. Idris, M. W. Uddin, "Numerical solution of both ends fixed deep beams," *Comput. Struct.*, vol. 61, no. 1, pp. 21-29, Aug. 1996.
[13] S. R. Ahmed, M. R. Khan, K. M. S. Islam, M. W. Uddin, "Investigation of stresses at the fixed end of deep cantilever beams," *Comput. Struct.*, vol. 69, no. 3, pp. 329-338, Nov. 1998.
[14] W.X. Zhong, X.S. Xu, H.W. Zhang, "On a direct method for the problem of elastic curved beams," *Eng. Mech.*, vol. 13, no. 4, pp.1-8, Nov. 1996. (In Chinese)
[15] R. D. Cook, "Axisymmetric finite element analysis for pure moment loading of curved beams and pipe bends," *Comput. Struct.*, vol. 33, no. 2, pp. 483-487, Oct. 1989.
[16] N. Rattanawangcharoen, H. Bai, A. H. Shah, "A 3D cylindrical finite element model for thick curved beam stress analysis," *Int. J. Numer. Meth. Eng.*, vol. 59, no. 4, pp. 511-531, Jan. 2004.
[17] T. H. Richards, M. J. Daniels, "Enhancing finite element surface stress predictions: A semi-analytic technique for axisymmetric solids," *J. Strain Anal. Eng. Des.*, vol. 22, no. 2, pp. 75-86, Apr. 1987.
[18] J. Smart, "On the determination of boundary stresses in finite elements," *J. Strain Anal. Eng. Des.*, vol. 22, no. 2, pp. 87-96, Apr. 1987.
[19] P. Gangan, "The curved beam/deep arch/finite ring element revisited," *Int. J. Numer. Meth. Eng.*, vol. 21, no. 3, pp. 389-407, Mar. 1985.
[20] J. O. Dow, M. S. Jones, S. A. Harwood, "A new approach to boundary modeling for finite difference applications in solid mechanics," *Int. J. Numer. Meth. Eng.*, vol. 30, no. 1, pp. 99-113, Jul. 1990.
[21] G. Ranzi, F. Gara, M. A. Bradford, "Analysis of composite beams with partial shear interaction using available modeling techniques: A comparative study," *Comput. Struct.*, vol. 84, no. 13-14, pp. 930-941, May 2006.
[22] S. R. Ahmed, M. Z. Hossain, M. W. Uddin, "A general mathematical formulation for finite-difference solution of mixed-boundary-value problems of anisotropic materials," *Comput. Struct.*, vol. 83, no.1,pp. 35-51, Jan. 2005.
[23] J. Chen, W. Cheng, G. Wang, H. Li, and Y. Li, "New method of monitoring the transmission range of coal seam water injection and correcting the monitoring results," *Measurement*, vol. 177, pp. 109334-1–109334-16, Jun. 2021.
[24] H. Yang, W. M. Cheng, Z. Liu, W. Y. Wang, D. W. Zhao, W. D. Wang, "Fractal characteristics of effective seepage channel structure of water infusion coal based on NMR experiment," *Rock and Soil Mechanics*, vol. 41, no. 4, pp. 1279-1286, Apr. 2020. (In Chinese)
[25] G. Wang, J. Z. Li, Z. Y. Liu, X. J. Qin, S. Yan, "Relationship between wave speed variation and microstructure of coal under wet conditions," *Int. J. Rock Mech. Min. Sci.*, vol. 126, pp. 104203-1–104203-11, Feb. 2020.